

Existence of collisional trajectories of Mercury, Mars and Venus with the Earth

J. Laskar¹ & M. Gastineau¹

It has been established that, owing to the proximity of a resonance with Jupiter, Mercury's eccentricity can be pumped to values large enough to allow collision with Venus within 5 Gyr (refs 1–3). This conclusion, however, was established either with averaged equations^{1,2} that are not appropriate near the collisions or with non-relativistic models in which the resonance effect is greatly enhanced by a decrease of the perihelion velocity of Mercury^{2,3}. In these previous studies, the Earth's orbit was essentially unaffected. Here we report numerical simulations of the evolution of the Solar System over 5 Gyr, including contributions from the Moon and general relativity. In a set of 2,501 orbits with initial conditions that are in agreement with our present knowledge of the parameters of the Solar System, we found, as in previous studies², that one per cent of the solutions lead to a large increase in Mercury's eccentricity—an increase large enough to allow collisions with Venus or the Sun. More surprisingly, in one of these high-eccentricity solutions, a subsequent decrease in Mercury's eccentricity induces a transfer of angular momentum from the giant planets that destabilizes all the terrestrial planets ~ 3.34 Gyr from now, with possible collisions of Mercury, Mars and Venus with the Earth.

Owing to chaotic behaviour of the Solar System^{4–7}, the distance between two initially close orbital solutions increases by a factor of ten every ten million years^{4,7,8}. It is thus hopeless to search for a precise solution for the motion of the Solar System over 5 Gyr, that is, over a time comparable to its age or life expectancy (before the Sun becomes a red giant). The most precise long-term solutions for the orbital motion of the Solar System are not valid over more than a few tens of millions of years^{9,10}. A numerical integration of the Solar System's motion over 5 Gyr can thus only be considered as a random sample of its possible evolution. Statistical studies are then required to search for possible changes in the planetary orbits that lead to collisions or disruption of the system.

The first study of the planetary orbits over several billion years was obtained after averaging the equations of motion over the fast orbital motion of the planets, which allowed a decrease in integration time of three orders of magnitude¹. This study revealed the possibility of Mercury's eccentricity reaching very high values, allowing collisions with Venus in less than 5 Gyr. However, this method has the drawback that the averaged equations are no longer justified in the vicinity of a collision. Despite the increase in computational power, recent integrations on gigayear timescales still neglected the relativistic contribution^{2,3,11}. The study of the full Solar System using general relativity and non-averaged equations on gigayear timescale thus needed to be done.

The model for the integration of the planetary orbits is derived from the La2004 model⁹ that was integrated over 250 Myr for the study of the palaeoclimates of the Earth and Mars^{9,12}. It comprises the eight major planets and Pluto and includes relativistic¹³ and averaged

lunar contributions¹⁴ (Supplementary Information). We used the SABA4 symplectic integrator¹⁵, which is adapted to perturbed Hamiltonian systems. The step size is 2.5×10^{-2} years, unless the eccentricity of the planets increases beyond about 0.4, in which case the step size is reduced to preserve numerical accuracy.

In a first experiment performed without the Moon or relativistic contributions, we integrated the equations over 5 Gyr for 201 orbits with the same initial conditions, except for an offset of 3.8 km ($k \in [-100, 100]$) in the semi-major axis of Mercury (its actual uncertainty is of a few metres (refs 16, 17)). In 60% of the solutions, we observed large increases in Mercury's eccentricity, beyond 0.9 (Fig. 1a). The statistics (Supplementary Table 1a) are comparable to the results of the non-relativistic secular equations². Among the 121 solutions of large eccentricity ($e > 0.7$), 34 ended in collision with

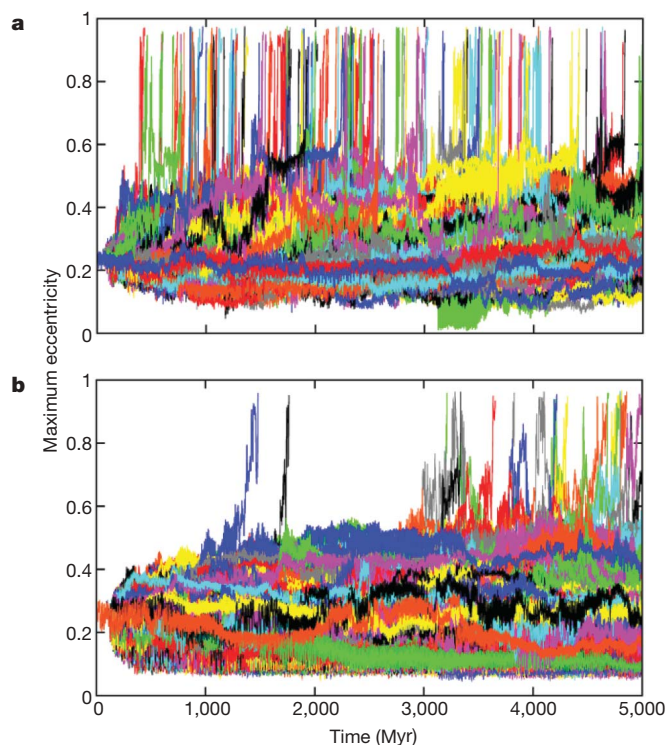


Figure 1 | Mercury's eccentricity over 5 Gyr. Evolution of the maximum eccentricity of Mercury (computed over 1-Myr intervals) over 5 Gyr. **a**, Pure Newtonian model without the contribution of the Moon, for 201 solutions with initial conditions that differ by only 3.8 cm in the semi-major axis of Mercury. **b**, Full Solar System model with relativistic and lunar contributions, for 2,501 solutions with initial conditions that differ by only 0.38 mm in the semi-major axis of Mercury.

¹Astronomie et Systèmes Dynamiques, IMCCE-CNRS UMR8028, Observatoire de Paris, UPMC, 77 Avenue Denfert-Rochereau, 75014 Paris, France.

the Sun, 86 in collision with Venus and a single one reached the 5-Gyr limit before collision.

According to the secular analysis², we could expect a much smaller number of collisional orbits in the full relativistic model. To estimate the probabilities of large eccentricity deviations in the relativistic model, we thus had to increase the scale of the numerical experiment. Using the JADE supercomputer at the French National Computing Centre CINES, we integrated 2,501 orbital solutions, S_k , of the complete model over 5 Gyr, with the initial semi-major axis of Mercury differing by 0.38 kmm ($k \in [-1,250, 1,250]$) from that in the nominal solution, S_0 , which was adjusted to the planetary ephemeris INPOP06¹⁷. The results (Fig. 1b and Supplementary Table 1b) are comparable to those of the relativistic secular equations², with Mercury having a high eccentricity in about 1% of solutions.

Among these 2,501 solutions that are compatible with our best knowledge of the Solar System, in 20 the eccentricity of Mercury increased beyond 0.9. At the time of writing, 14 of these have not yet reached 5 Gyr and may still be running for a few months, as their step size is greatly reduced. Solution S_{-947} reached 5 Gyr without collision, although a close encounter (closest approach, 6,500 km) occurred between Mercury and Venus at 4.9 Gyr. In S_{-915} , S_{-210} and S_{33} , Mercury collided with the Sun at 4.218, 4.814 and 4.314 Gyr, respectively, whereas in S_{-812} , Mercury collided with Venus at 1.763 Gyr. The most notable solution is S_{-468} , in which a close encounter of Mars with the Earth with a closest approach of only 794 km occurs at 3.3443 Gyr (Fig. 2). Such a close approach would be disastrous for life on the Earth, with a possible tidal disruption of Mars and subsequent multiple impacts on the Earth^{18,19}, but we also searched for more direct collisions. We integrated 201 different versions, $S_{-468}^{(k)}$ ($k \in [-100, 100]$), of S_{-468} , starting at 3.344298 Gyr,

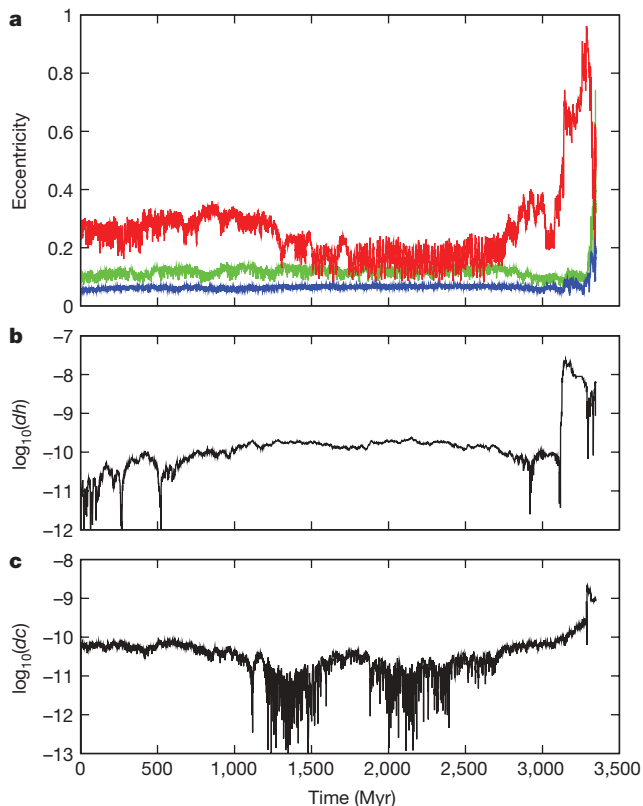


Figure 2 | Example of collisional trajectory for Mars and the Earth. **a**, Evolution of the maximum eccentricity of Mercury (red), Mars (green) and the Earth (blue), recorded over 1-Myr intervals for the solution $S_{-468}^{(-15)}$. **b, c**, Relative variation, dh , of the total energy of the system (**b**) and total angular momentum, dc (**c**), on a logarithmic scale. During the whole integration, the relative variations of the total energy and angular momentum of the system remain below 2.3×10^{-8} and 2.2×10^{-9} , respectively.

each with an offset of 0.15 kmm in the semi-major axis of Mars. Within 100 Myr, five cases lead to the ejection of Mars from the Solar System (semi-major axis >100 AU) and the remaining 196 solutions end in collision, with the following distribution: Sun–Mercury, 33; Sun–Mars, 48; Mercury–Venus, 43; Mercury–Earth, 1; Mercury–Mars, 1; Venus–Earth, 18; Venus–Mars, 23; Earth–Mars, 29.

The most surprising collision is the one of Venus with the Earth, which occurs in $S_{-468}^{(-1)}$ in a five-stage process (Figs 2 and 3). The first step is the increase in the eccentricity of Mercury, obtained through perihelion resonance with Jupiter^{2,3} at 3.137 Gyr. This step is essential, as it allows a transfer of non-circular angular momentum from the outer planets to the terrestrial planets²⁰. The eccentricity increase of Venus, the Earth and Mars, is then obtained through secular resonances among the inner planets while the eccentricity of Mercury decreases between 3.305 and 3.325 Gyr. Once Mars and the Earth acquire large eccentricities, close encounters occur and collisions become possible, as in $S_{-468}^{(-15)}$ (Fig. 3c). In $S_{-468}^{(-1)}$, the collision with Mars does not occur, but several close encounters (Fig. 3c) lead to the

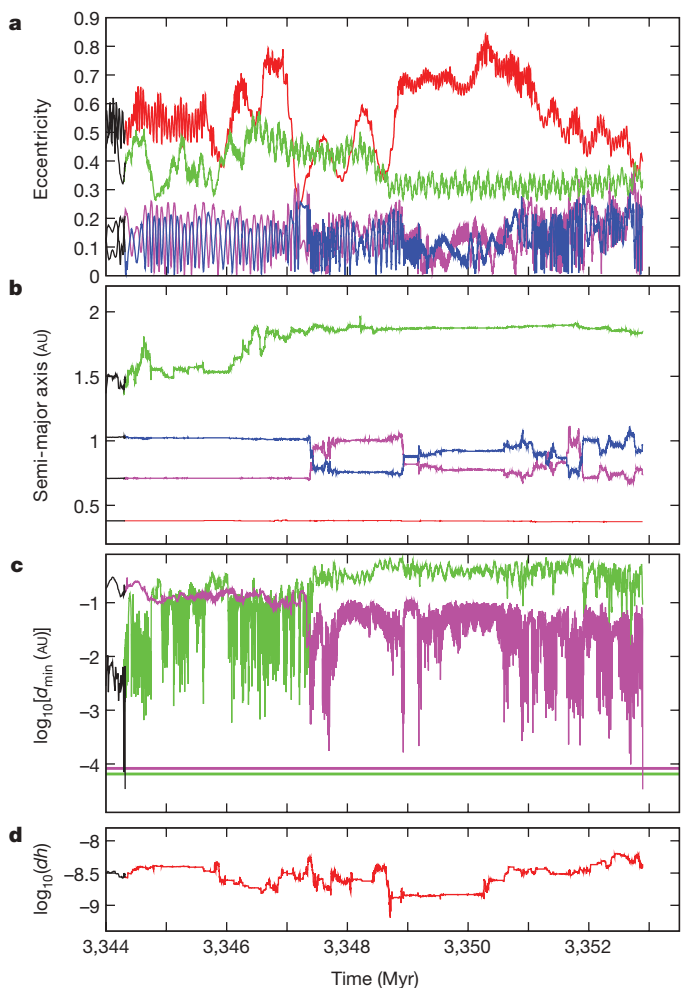


Figure 3 | Collisional trajectories for Mars and Venus with the Earth. The two solutions, $S_{-468}^{(-15)}$ (black) and $S_{-468}^{(-1)}$ (colours), are identical until 3.344298 Gyr. At this time, an offset of 0.15 kmm is applied to the semi-major axis of Mars in the solution $S_{-468}^{(k)}$. **a, b**, Eccentricity (**a**) and semi-major axis (**b**) plotted versus time for Mercury (red), Venus (pink), the Earth (blue) and Mars (green). **c**, Minimum Earth–Mars (green) and Earth–Venus (pink) distances in astronomical units, recorded over each 1,000-yr time interval. The horizontal lines are the Mars–Earth (6.5322×10^{-5} AU, green) and Venus–Earth (8.30827×10^{-5} AU, pink) distances of collision, d_{\min} , corresponding to the sum of the planets' radii. For $S_{-468}^{(-15)}$, the Earth–Mars distance reached at 3.344317 Gyr is 3.7752×10^{-5} AU, and for $S_{-468}^{(-1)}$, the Earth–Venus distance reached at 3.352891 Gyr is 3.3791×10^{-5} AU. **d**, Relative energy variation.

diffusion of Mars's semi-major axis (Fig. 3b) until secular resonances produce a decrease in the eccentricity of Mercury together with an additional increase in the eccentricity of Venus and the Earth at about 3.347.3 Gyr (Fig. 3c). At this point, close encounters between Venus and the Earth occur, with several exchanges of the planets' orbits (Fig. 3b) before a final collision at 3.352891 Gyr (Fig. 3c).

The essential trigger for the collisional trajectories of Mars and Venus with the Earth is the great increase in Mercury's eccentricity. If this increase leads rapidly to a collision with the Sun or with Venus, as in S_{33} and S_{-812} , the remaining part of the Solar System is not much affected; these two solutions, after merging of the colliding bodies, are actually very stable when extended to 5 Gyr. We expect that this will be the case for most of the solutions in which Mercury has high eccentricity. However, in some less frequent events, such as S_{-468} , the eccentricity increase of Mercury leads to a total destabilization of the inner Solar System. In the simulations described here, we restricted the initial conditions to a very small neighbourhood, assuming that the chaotic behaviour of the system will randomize the initial conditions. The fact that the probability distribution of Mercury's eccentricity (Supplementary Table 1) is very similar to the results obtained with the averaged equations and a much more widely distributed set of initial conditions² leads us to propose that the probability of a large increase in the eccentricity of Mercury is about 1%. It remains difficult to evaluate the probability of a collision involving the Earth within 5 Gyr. Indeed, although we studied variations around solution S_{-468} that lead to collision with the Earth in about 25% of the cases, the S_{-468} orbit is essentially the single event of its kind in our full sample of 2,501 solutions.

Received 17 February; accepted 22 April 2009.

- Laskar, J. Large scale chaos in the Solar System. *Astron. Astrophys.* **287**, L9–L12 (1994).
- Laskar, J. Chaotic diffusion in the Solar System. *Icarus* **185**, 312–330 (2008).
- Batygin, K. & Laughlin, G. On the dynamical stability of the Solar System. *Astrophys. J.* **683**, 1207–1216 (2008).
- Laskar, J. A numerical experiment on the chaotic behaviour of the Solar System. *Nature* **338**, 237–238 (1989).
- Laskar, J. The chaotic motion of the Solar System. A numerical estimate of the size of the chaotic zones. *Icarus* **88**, 266–291 (1990).
- Laskar, J., Quinn, T. & Tremaine, S. Confirmation of resonant structure in the Solar System. *Icarus* **95**, 148–152 (1992).
- Sussman, G. J. & Wisdom, J. Chaotic evolution of the Solar System. *Science* **257**, 56–62 (1992).
- Laskar, J. The limits of Earth orbital calculations for geological time scale use. *Phil. Trans. R. Soc. Lond. A* **357**, 1735–1759 (1999).
- Laskar, J. et al. A long term numerical solution for the insolation quantities of the Earth. *Astron. Astrophys.* **428**, 261–285 (2004).
- Varadi, F., Runnegar, B. & Ghil, M. Successive refinements in long-term integrations of planetary orbits. *Astrophys. J.* **592**, 620–630 (2003).
- Ito, T. & Tanikawa, K. Long-term integrations and stability of planetary orbits in our Solar System. *Mon. Not. R. Astron. Soc.* **336**, 483–500 (2002).
- Laskar, J. et al. Long term evolution and chaotic diffusion of the insolation quantities of Mars. *Icarus* **170**, 343–364 (2004).
- Saha, P. & Tremaine, S. Long-term planetary integration with individual time steps. *Astron. J.* **108**, 1962–1969 (1994).
- Boué, G. & Laskar, J. Precession of a planet with a satellite. *Icarus* **196**, 1–15 (2008).
- Laskar, J. & Robutel, P. High order symplectic integrators for perturbed Hamiltonian systems. *Celest. Mech. Dynam. Astron.* **80**, 39–62 (2001).
- Standish, M. An approximation to the errors in the planetary ephemerides of the Astronomical Almanac. *Astron. Astrophys.* **417**, 1165–1171 (2004).
- Fienga, A., Manche, H., Laskar, J. & Gastineau, M. INPOP06: a new numerical planetary ephemeris. *Astron. Astrophys.* **477**, 315–327 (2008).
- Holsapple, K. A. & Michel, P. Tidal disruptions: a continuum theory for solid bodies. *Icarus* **183**, 331–348 (2006).
- Asphaug, E., Agnor, C. B. & Williams, Q. Hit-and-run planetary collisions. *Nature* **439**, 155–160 (2006).
- Laskar, J. Large scale chaos and the spacing of the inner planets. *Astron. Astrophys.* **317**, L75–L78 (2007).

Supplementary Information is linked to the online version of the paper at www.nature.com/nature.

Acknowledgements This work benefited from support from the Planetology Programme of the French National Research Centre, from Paris Observatory and from National Research Agency grant ASTS-CM. The authors thank the computing centres of Paris Observatory, the Institut de Physique du Globe Paris, the Institute of Development and Resources in Scientific Computing, the Linear Accelerator Laboratory Grid and especially the French National Computing Centre CINES, for providing the necessary computational resources for this work.

Author Contributions J.L. designed the study, performed the simulations and their analysis, and wrote the paper. M.G. wrote the computer code.

Author Information Reprints and permissions information is available at www.nature.com/reprints. Correspondence and requests for materials should be addressed to J.L. (laskar@imcce.fr).

SUPPLEMENTARY INFORMATION

(a) Without GR							
e_{m0}	500	1000	1500	2000	3000	4000	5000
0.35	164	423	537	627	766	826	886
0.40	80	313	443	527	667	736	831
0.50	25	124	209	333	517	612	687
0.60	15	95	169	274	433	547	612
0.70	15	90	154	264	423	527	602
0.80	15	90	149	259	423	527	602
0.90	10	85	149	259	423	527	602

(b) With GR							
e_{m0}	500	1000	1500	2000	3000	4000	5000
0.35	30	91	143	202	318	418	492
0.40	3	20	39	67	126	189	255
0.50	0	0	1	3	10	20	40
0.60	0	0	0	1	2	5	10
0.70	0	0	0	1	1	4	9
0.80	0	0	0	1	1	4	8
0.90	0	0	0	1	1	3	8

Table 1: Probability ($\times 1000$) for the eccentricity of Mercury (e_{max}) to reach a given value (e_{m0}) over a given time (500, 1000, 1500, 2000, 3000, 4000, 5000 Myr). Top: without general relativity. The statistics are made over 201 orbital solutions that differ from 3.8 cm in the initial value of Mercury's semi-major axis. Bottom: with general relativity. The statistics are made over 2501 orbital solutions that differ from 0.38 mm in the initial value of Mercury's semi-major axis.

The numerical model

The model for the integration of the planetary orbits comprises the 8 major planets and Pluto with relativistic and lunar contributions. In order to speed up the integrations, the Lunar contributions have been averaged over the Lunar mean longitude and longitude of perihelion[14]. In addition, a small model of the tidal dissipation in the Earth Moon System has been derived, providing a realistic evolution of the Earth-Moon distance and of the rotation speed of the Earth over 5 Gyr. This model has been adjusted to the La2004 solution[9] over 250 Myr and fitted with a three parameters formula

$$a = a_0(1 + a_1/\alpha T + a_2 T^2)^\alpha \quad (1)$$

where a_0 is the Earth-Moon semi-major axis at the origin of time (J2000), T is in Gyr, and $\alpha = 0.113381622646105$; $a_2 = -0.0178457555910623$; $a_1 = 0.101773133860118$. The evolution of the spin rate of the Earth is then derived from the conservation of angular momentum. These tidal terms induce a small dissipation in the total energy of the Solar system that is taken into account in order to monitor the precision of the numerical integration[9].

The relativistic equations are the same as in La2004[9] and derive from an Hamiltonian formulation of Saha and Tremaine[13]. The quadrupole contribution of the Sun is taken into account with $J_2 = 2 \times 10^{-7}$. In order to speed up computation, the integrations are performed in standard double precision arithmetic and not in extended precision as in ref[2]. The stepsize is 2.5×10^{-2} years, unless the eccentricity of the planets increases beyond about 0.4, in which case the step size is reduced to preserve numerical accuracy. In order to limit the possible drift of energy that can result from repeated increase of the step size in symplectic integrators, we keep the step size constant over time intervals of 12.5 yr, which results in a satisfactory conservation of the energy (Fig. 2b).

The average integrations time are of about 2500 h per run on a Xeon 5472 CPU core, while the total CPU time for the whole study exceeded 6 million hours. For a better tracking of the energy and angular momentum, we have not taken into account the mass loss of the Sun. We have not considered either the tidal deformation of the bodies during close encounters and their possible tidal disruption[18, 19].

The initial conditions are obtained by a fit over the solution of the more complete model INPOP06[17]. In order to compensate for the lack of asteroid contribution, we have added a small constant term to the precessional motion of the planetary orbits, resulting from a fit of the long time solution over a version of INPOP06 that has been extended over 1 Myr in the past (Table 2). As a check of the resulting model, the differences in eccentricity and inclination between the present solution and INPOP06[17] are given over the interval $[0, +1\text{Myr}]$ (Table 3). The derived initial conditions are in Table 4, while all the other parameters are from INPOP06[17].

planet	dg	ds
Mercury	-0.001683033	0.000853116
Mars	0.000365005	-0.000203123
Jupiter	0.000015692	0.000006453

Table 2: Corrections (in arcsec/yr) in the perihelion velocity (dg) and in the node velocity (ds) for Mercury, Mars, and Jupiter. The main effect of these terms is to correct for the absence of asteroids in the model.

planet	$\Delta a \times 10^6$ (AU)	$\Delta e \times 10^6$	$\Delta i \times 10^6$ (rad)
Mercury	0.01	7.61	2.51
Venus	0.05	6.05	1.73
Earth	0.09	4.59	1.36
Mars	0.56	4.39	2.03
Jupiter	0.35	1.52	0.22
Saturn	3.61	2.84	0.19
Uranus	6.24	1.32	0.08
Neptune	4.79	0.20	0.06
Pluto	16.06	0.22	0.09

Table 3: Maximum difference in semi-major axis (Δa), eccentricity (Δe) and inclination in radians (Δi) for the different planets over the time interval $[0, +1\text{Myr}]$, compared to INPOP06[17]. The solution has been adjusted to INPOP06[17] over the time interval $[-1\text{Myr}, 0]$. The solution for the Earth is compared to the Earth–Moon barycenter of INPOP06.

body	X	Y	Z
Mer	-1.3723006138719493E-01	-4.0324074993791997E-01	-2.0141230251495065E-01
Ven	-7.2543875164004101E-01	-4.8921282357574918E-02	+2.3717655135959591E-02
EMB	-1.8429523869857883E-01	+8.8475982513797391E-01	+3.8381372854387652E-01
Mar	+1.3835794659467666E+00	-1.2458187406789204E-03	-3.7883156713073539E-02
Jup	+3.9940405805302190E+00	+2.7339319131097417E+00	+1.0745892889690563E+00
Sat	+6.3992728946824826E+00	+6.1720105115817834E+00	+2.2738481118833267E+00
Ura	+1.4424722672081669E+01	-1.2508913521035904E+01	-5.6826123000986799E+00
Nep	+1.6804916776997999E+01	-2.2982754337214441E+01	-9.8253491124291390E+00
Plu	-9.8824902214449857E+00	-2.7981516729922184E+01	-5.7546154515900296E+00
Sun	-7.1364558632045867E-03	-2.6470343693797828E-03	-9.2298925054966601E-04
Moo	-1.9492816871869883E-03	-1.7828918671608514E-03	-5.0871368540258022E-04
body	DX	DY	DZ
Mer	+2.1371774109527775E-02	-4.9330576077080499E-03	-4.8504663887848996E-03
Ven	+8.0349594196834088E-04	-1.8498595723320826E-02	-8.3727680942960545E-03
EMB	-1.7197730598869702E-02	-2.9096001847899629E-03	-1.2615424684121190E-03
Mar	+6.7687800264027093E-04	+1.3807279327919367E-02	+6.3148675769632316E-03
Jup	-4.5629353241739114E-03	+5.8747038486458630E-03	+2.6292698127070692E-03
Sat	-4.2869731379417009E-03	+3.5215868716827110E-03	+1.6388979154519450E-03
Ura	+2.6834835473886366E-03	+2.4552463507823063E-03	+1.0373752265128999E-03
Nep	+2.5846532680459892E-03	+1.6616665134371927E-03	+6.1578095014691201E-04
Plu	+3.0341305844833063E-03	-1.1343440334706748E-03	-1.2681632917206367E-03
Sun	+5.3784605099164219E-06	-6.7581880103245664E-06	-3.0328531274874777E-06
Moo	+3.7167046671156826E-04	-3.8469783519282943E-04	-1.7403015998408315E-04

Table 4: Initial conditions for the positions (X, Y, Z) and velocities (DX, DY, DZ), of the Sun, the planets and the Moon at J2000 in the ICRF reference frame, for the nominal solution S_0 . Units are AU and AU/days.